Organized Silica Microspheres Carrying Ferromagnetic Cobalt Nanoparticles as a Basis for Tip Arrays in Magnetic Force Microscopy

Sivarajan Ramesh,[†,§] Yair Cohen,[†] Ruslan Prozorov,[‡] Kurikka V. P. M. Shafi,[†] Doron Aurbach,[†] and Aharon Gedanken*[,†]

Department of Chemistry and Department of Physics, Bar-Ilan University, Ramat Gan 52900, Israel

Received: June 18, 1998; In Final Form: August 17, 1998

Two-dimensional arrays of hard spherical particles carrying a nanoprobe hold potential as scanning tip arrays (STA) in force microscopy. Though rigid single molecules of proteins were originally envisioned as suitable probes, we foresee the possibility that magnetic nanoparticles, as well, could qualify the criteria. Ferromagnetic cobalt nanoparticles of size ∼10 nm well adhered to hard silica microspheres (225−250 nm) were synthesized by the sonochemical decomposition of a volatile organic precursor cobalt nitrosyl carbonyl [$Co(CO)_3NO$] in a suspension of silica in Decalin, followed by crystallization of the resultant amorphous produt. The morphological, thermal, and magnetic properties of the amorphous and nanocrystalline cobalt particles adhered to the microspherical silica were investigated by XRD, TEM, SEM/EDAX, TGA, DSC, EPR and magnetic susceptibility methods. Silica spheres carrying ferromagnetic cobalt nanocrystals were deposited on a single crystalline silicon ⟨100⟩ substrate by spin coating. The two-dimensional organization of the magnetic microspheres on silicon and the adhesion of cobalt nanoparticles on the surface of microspherical silica have been examined by scanning electron microscopy and atomic force microscopy (AFM), respectively. While the system described here forms only a basis for a functioning device, a chemical approach toward the synthesis, evaluation, and assembly of the components is emphasized.

Introduction

The tendency of monodispersed particles in a suspension to form ordered arrays is influenced by the nature of the interaction exhibited by the particles with the molecules of the dispersant and among themselves. This property is an important parameter in the fabrication of organized nanostructures by self-assembly (SA) or Langmuir−Blodgett (LB) techniques[1] and has been exploited to form ordered arrays of a range of nanoparticles such as ceramics, metals, and polymers.[2] Tapping the self-organizing nature of the particles to form ordered arrays with specific properties on single crystalline substrates turns out to be a worthy and logical goal. For the same reason, the chemical forces directing the self-organization of monodispersed spherical particles in dilute suspensions have attracted theoretical research attention as well.[3] Such an assembly of nanoparticles has been shown to form the basis for the fabrication of lithographic masks from an array of polystyrene spheres,[4] ultramicroelectrodes from gold nanoparticles,[5] chemical sensors, and switchable optical diffraction devices from a crystalline colloidal array of particles in polyacrylamide hydrogel.[6] Organized array of microspherical objects have recently emerged as an alternative to organic surfactants as templating agents in the design and synthesis of macroporous solids.[7]

In recent years scanning force microscopy has emerged as a powerful tool to measure magnetic and atomic forces in nanodimensions.[8,9] Magnetic force microscopy (MFM) involves the interactions between a magnetic tip and a sample surface, quantified by the regular deflection system employed in atomic force microscopy.[8] The force derivative (F) for a pyramidal magnetic tip (of saturation magnetization M_t) acting on a sample of saturation magnetization M_s is denoted by the expression[9]

$$F = 2w\mu_o M_s M_t [\tan^2(\theta/2)/\cosh(qx/\delta)]\zeta \qquad (1)$$

where μ_o is the magnetic permeability of the medium, θ is the angle of the pyramid, q is a parameter related to the magnetocrystalline anisotropy (H_k) as $q = \sqrt{(M_s/2H_k)^{1/2}}$, δ is the ferromagnetic exchange length, w is the wall width, and ζ is a parameter expressed as a series in terms of the tip height, l, and w. Though the force derivative is directly proportional to the saturation magnetization of the probing tip, theoretical studies have stressed the importance of the geometry of the scanning probe, where a magnetic tip could function efficiently.[10]

Drexler recently proposed[11] a geometry wherein spherical particles carrying nanometer scale probes, organized on flat substrates could act as "tip arrays" capable of making force measurements in high resolutions. A possible geometry for such a tip array originally proposed by Drexler is shown schematically in Figure 1, where the larger sphere is a primary bead and the secondary beads comprise of an array of smaller spherical particles. Drexler expressed the diameter of the scan area to be

$$d = (8(2h - \delta)(r_1 + r_2) r_1/r_2)^{1/2} \qquad (2)$$

where h is the height of the probe tip and δ is the minimum imaging separation as shown in Figure 1. Though single and rigid macromolecules, such as proteins and DNA, were originally proposed to be used as probe tips by Drexler and Foster[12]

* To whom correspondence should be addressed. E-mail: gedanken@ashur.cc.biu.ac.il. Tel: 0972-3-5358315. Fax: 0972-3-5351250.
[†] Department of Chemistry.
[‡] Department of Physics.
[§] Current address: Department of Materials Science and Engineering, Bard Hall, Cornell University, Ithaca, NY 14853.

10.1021/jp982684r CCC: $15.00
Published on Web 11/13/1998

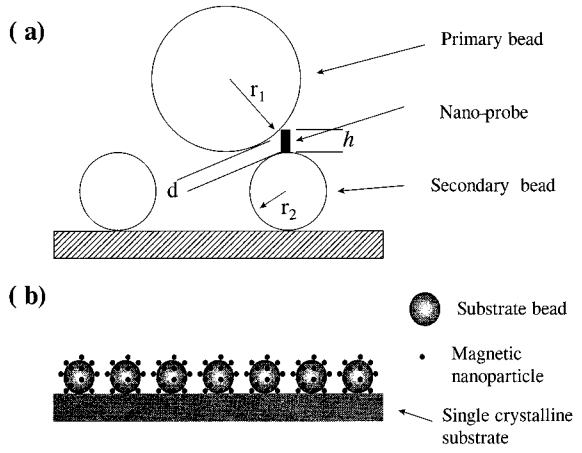

Figure 1. (a) Schematic arrangement of a tip-array geometry proposed by Drexler (see ref 11). The larger sphere (radius r_1) is a primary bead and the secondary beads comprise of an array of smaller spherical particles (radius r_2). The diameter of the scan area is given by $d = (8(2h - \delta)(r_1 + r_2)r_1/r_2)^{1/2}$. (b) Schematic diagram of an array of spherical beads carrying uniform magnetic nanoparticles.

to measure biological interactions, we foresee a possibility that uniform magnetic nanoparticles in the size range of 5−10 nm strongly adhering to spherical bead surfaces can likewise function as probe tips to measure the magnetic forces of interactions. A schematic diagram of such an array is shown in Figure 1b.

Meeting such an objective involves (a) the synthesis of magnetic nanoparticles and spherical substrate beads in appropriate dimension, (b) the uniform deposition of the magnetic nanoparticles on to the surface of substrate beads, and (c) the organization of the beads carrying magnetic nanoparticles on an atomically flat substrate.

The sonochemical methods employing power ultrasound readily qualify for this task due to the ability to combine the synthesis of a variety of magnetic nanoparticles[13] and their deposition on spherical substrates in a single operation.[14] Ultrasound cannot effect chemical changes by directly coupling with molecular vibrations. Rather, its ability to direct the course of chemical reaction stems from acoustic cavitation involving the formation, oscillatory growth, and implosive collapse of bubbles in a liquid medium.[15]

Stober's silica submicrospheres,[16] obtained by the base-catalyzed hydrolysis of Tetraethyl orthosilicate (TEOS), qualify as suitable hard spherical substrates for the following reasons: (a) a narrow size distribution can be achieved over a wider range, (b) their surface silanol composition and extent of hydrogen bonding can be modified by thermal treatments to change the reactivity, (c) the ability of the reactive silanol groups to form covalent links with supramolecular organic moieties, and (d) the isotropic interactions in an aqueous or organic suspension which help to form ordered arrays on substrates. With a continuing interest in the controlled synthesis and characterization of ceramic and metal−ceramic nanoparticles, we have explored the effect of power ultrasound on ceramic materials such as silica microbeads and alumina gel,[17] the deposition of various magnetic nanoparticles, such as nickel[15] and iron/ iron oxides,[18] on the surface of submicrospherical silica and the nature of adhesion in the metal particle−spherical silica interface.[19]

In this paper we describe the synthesis of silica microspheres carrying ferromagnetic cobalt nanoparticles, their morphological, thermal, magnetic, and interfacial properties. Monolayer arrays of the silica spheres carrying cobalt nanoparticles were obtained on a single crystalline silicon Si ⟨100⟩ surface by spin coating. The array of microspheres and the adhesion of cobalt nanoparticles to the spherical silica surface have been studied by scanning electron microscopy (SEM) and atomic force microscopy (AFM). Such an array of magnetic microspheres is proposed as a suitable tip array geometry to carry out magnetic force measurements. Although the system described here is far from being a functioning device, the potential of such an array to form the basis for a working device as well as a chemical approach toward the synthesis, evaluation, and assembly of the components is emphasized.

Experimental Section

(a) Materials. Cobalt nitrosyl carbonyl [$Co(CO)_3NO$] precursor was prepared by the nitrosylation of cobalt octacarbonyl [$Co_2(CO)_8$, Sigma] under flowing argon by a known procedure[20] and stored under argon. Amorphous submicrospheres of silica in the size range of 200−250 nm were synthesized by a base-catalyzed hydrolysis of tetraethyl orthosilicate (TEOS) described by Stober et al.[15] Silica microspheres thus obtained were washed extensively with alcohol and ether and dried under vacuum at room temperature.

(b) Sonochemical Deposition of Cobalt. Sonochemical deposition of amorphous cobalt was carried out as follows. A 250 mg amount of the silica sample was added to 40 mL of dry Decalin in a sonication cell, and the cell was attached to the sonicator horn under flowing argon. Argon gas was bubbled through the slurry for 1 h prior to sonication to expel any dissolved air/oxygen, and 0.25 mL of cobalt nitrosylcarbonyl was introduced into the slurry through a septum. Sonication of the slurry with a high-intensity ultrasound radiation for 1 h was carried out by employing a direct immersion titanium horn (Vibracell, 20 kHz, 100 W/cm^2) under flowing argon. The resulting products were washed with dry *n*-pentane inside a glovebox (O_2 < 10 ppm), thoroughly dried in vacuum, and stored under argon. Crystallization of the as prepared product was carried out by heating a small amount of sample in a glass vial at a temperature of 400 °C under flowing argon for 3 h.

(c) Characterization. X-ray diffraction of the solid products was carried out on a Rigaku X-ray diffractometer (Model-2028, Cu Kα) on small amounts of sample material placed on a glass plate and covered with a protective layer of collodion. The particle morphology and the nature of its adherence to silica were studied by transmission electron microscopy employing a JEOL-JEM 100SX microscope. Infrared spectra were recorded, employing a Nicolet (Impact 410) FT-IR spectrometer by a KBr disk method.

Thermogravimetric analysis (TGA) on the bare silica substrates and the cobalt covered silica samples were carried out employing a Mettler TG-50 instrument. The samples were heated to 900 °C at a rate of 10 °C/min under a flowing stream of nitrogen (50 cm^3/min). Differential scanning calorimetric (DSC) analysis of the samples in crimped aluminum crucibles was carried out up to a temperature of 450 °C, employing a Mettler equipment under a flowing stream of argon, also at a rate of 10 °C/min.

Magnetic susceptibility measurements at room temperature were carried out by employing a vibrating sample magnetometer on accurately weighed (ca. 10 mg) samples packed in a gelatin capsule under argon. Ferromagnetic resonance experiments at room temperature were run on a Bruker EMX instrument operating in the X-band.

(d) Organization on Si ⟨100⟩ and AFM Investigation. Single crystalline silicon ⟨100⟩ substrates measuring 6 mm × 6 mm × 0.5 mm were cleaned with nitric acid for inorganic

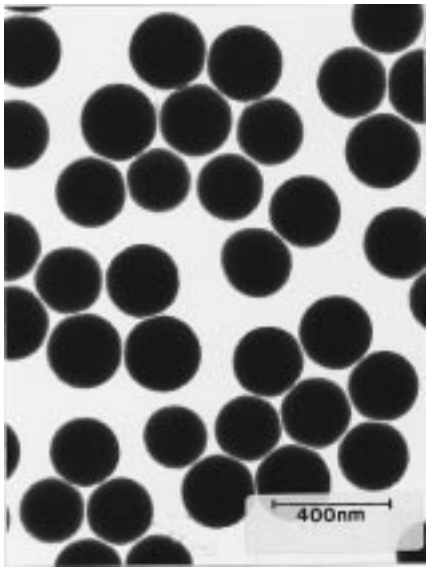

Figure 2. Transmission electron micrographs of the bare substrate silica microspheres.

impurities and with chloroform for any organic matter. Organization of the microspheres on the substrate was carried out employing a small custom-made spinning device. The silicon substrate was fastened flat on the horizontal rotating top (25 mm diameter) employing double-sided adhesive tape. Drops of a suspension of the cobalt coated silica spheres in ethanol was placed on the substrate during spinning. The deposition of the silica spheres in the absence of spinning resulted in heavy aggregation of the microspheres on the silicon surface. Silicon substrates coated with magnetic spheres were coated with ~400 Å of gold employing a Fisons sputtering equipment and analyzed by SEM. A closer examination of the array was also carried out by atomic force microscopy (AFM) on gold-coated samples because a thin layer of gold could limit the tip-induced sample movements on the silicon. The silicon sample was adhered to a stainless steel sample holder with a double-sided conducting carbon tape.

The nature of the interaction between the cobalt particles and the substrates was measured by carrying out AFM measurements on single silica microspheres embedded in a thermoplastic resin matrix. Sample preparation methods for this study have been discussed in detail elsewhere.[19] AFM investigations were carried out on a Topometrix Discoverer TMX 2010 atomic force microscope provided with a 70μm, tripodal, closed loop scanner with an built-in linearization system. Pyramidal silicon nitride tips (0.01 N/m, Park Scientific) in contact mode were employed for scanning at a frequency of about 7 Hz.

Results and Discussion

(a) Structural and Morphological Properties. The X-ray diffraction patterns of the as-prepared and crystallized samples of the amorphous silica microspheres deposited with cobalt nanoparticles showed no distinct diffraction peaks characteristic of cobalt. The transmission electron micrographs of the substrate silica microspheres used in the study are shown in Figure 2. The microspheres showed little size dispersion, with diameters in the range of 220−250 nm. The TEM micrograph of as prepared spherical silica particles deposited with amorphous cobalt are shown in Figure 3a. All the particles were uniformly covered with nanoclusters of cobalt. A single microsphere at a higher resolution is shown in Figure 3b. Small cobalt clusters in the size range of 2−3 nm completely covered

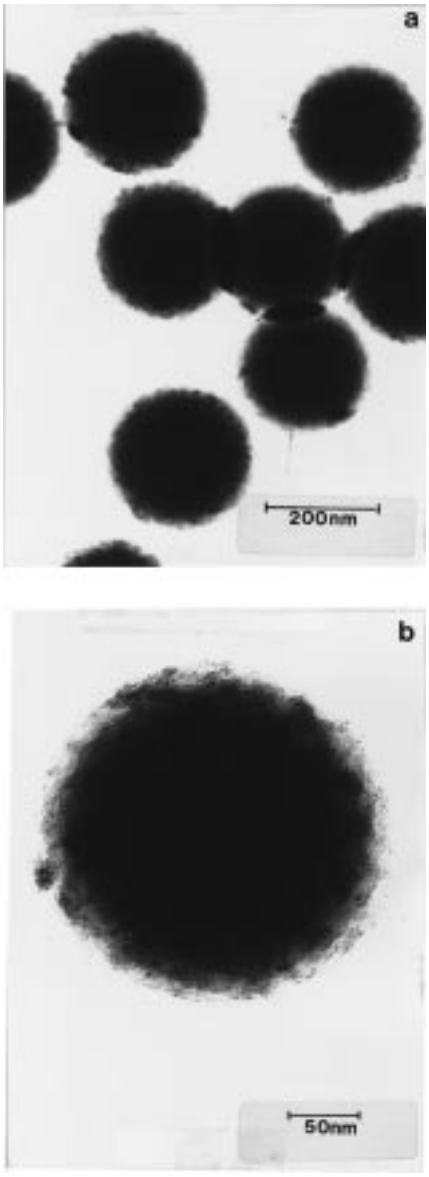

Figure 3. TEM micrograph of (a) as prepared spherical silica particles deposited with nanoclusters of amorphous cobalt (b) a single microsphere shown at a higher resolution.

the silica surface. The TEM micrographs of the crystallized samples are shown in Figure 4. The crystallization was also accompanied by sintering of the smaller amorphous clusters to spherical crystallites of about 10 nm diameter as can be seen from the micrograph. The elemental composition of the material was analyzed by EDAX, and the corresponding profiles for the as-prepared and crystallized samples are shown in Figure 5. The cobalt content in the case of the as-prepared and crystallized samples were 4.38% and 4.92%, respectively. Though the composition of lighter elements determined by EDAX could not be relied upon directly, oxygen content remained the same in the as-prepared and crystallized samples, ruling out oxidation of the small crystallites by external oxygen impurity during deposition or crystallization. As-prepared samples of cobalt coated on silica are expected to be amorphous due to the ultrafast cooling rates of more than 10^7 K/s encountered in the ultrasound driven process. The absence of well-defined X-ray diffraction lines in the case of the crystallized samples could be attributed only to their small sizes (ca. 10 nm) which could lead to extensive line broadening. When coupled with the presence of only ~4.9% of metallic cobalt in a background of amorphous

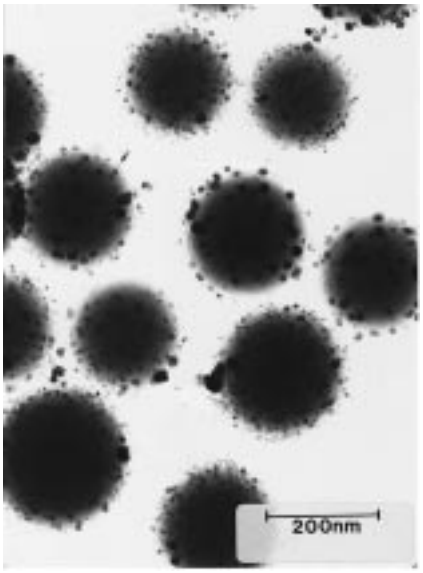

Figure 4. TEM micrograph of the spherical silica particles carrying nanocrystalline cobalt.

silica, the absence of Bragg diffraction lines is hardly surprising. For this reason the nature of the crystallinity of cobalt will be discussed in terms of the magnetic properties rather than in terms of the X-ray diffraction.

(b) Thermal Properties. The thermo gravimetric analysis (TGA) curve of the substrate silica microspheres and the as-prepared sample of cobalt-coated silica are shown in Figures 6a and b, respectively. The bare silica substrates showed a total weight loss of 16.57%, against a 24.68% loss in the case of cobalt-coated samples. Both of the samples showed two distinct regions of weight loss from 40 to 175 °C and 200−600 °C. Moreover, the cobalt-coated samples showed a further weight loss, accounting for a 2% loss in the temperature range of 600−780 °C. The DSC curves for the corresponding samples of bare silica substrates and the amorphous cobalt coated samples are shown in Figure 7. Both of the samples showed a broad endothermic peak in the region of 25−175 °C. The heat flow was about 2.5 times more in the case of bare silica than in the cobalt coated samples. However, the amorphous to crystalline transition of cobalt could not be detected in the DSC trace of the cobalt-coated sample.

The weight loss patterns in the case of the substrate silica and the cobalt-coated samples demand an understanding of the nature of thermally desorbable species on the surface of the silica spheres. The surface of the microspherical silica consists of a very small proportion of free silanols and silanols heavily hydrogen bonded among themselves and adsorbed water molecules.[21−23] The hydrogen bonded silanols show variations such as hydrogen bonding at the oxygen end, at the hydrogen end and at both ends. These thermally removable species are present on the walls of the inner pores as well. The population of the silanol and water molecules on the outer spherical surface of the particles is less than those present on the inner pore walls. The initial weight loss amounting to about 8% weight at lower temperature can be associated with desorbable species on the surface rather than on the inner pore walls. The initial weight loss in the temperature range of 40−175 °C can be associated with the breaking up of the hydrogen-bonded network and the expulsion of adsorbed water from the surface. The second stage of weight loss, in the range of 175−600 °C, could then be associated with the desorption of adsorbed water, as well as the water generated by the condensation of part of the free

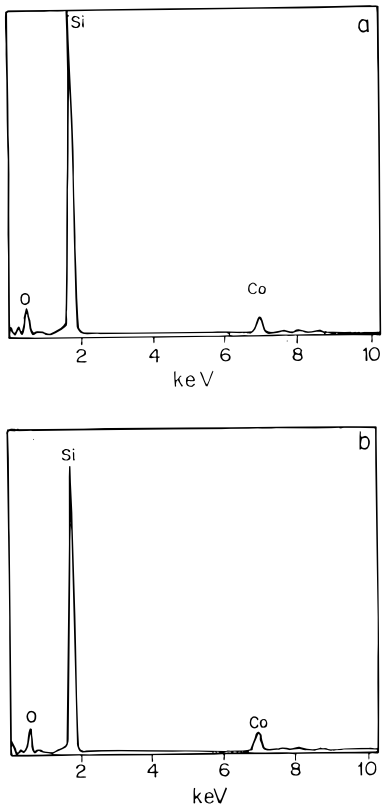

Figure 5. EDAX profiles showing the elemental composition of (a) as-prepared and (b) crystallized samples of spherical silica particles carrying nanophasic cobalt.

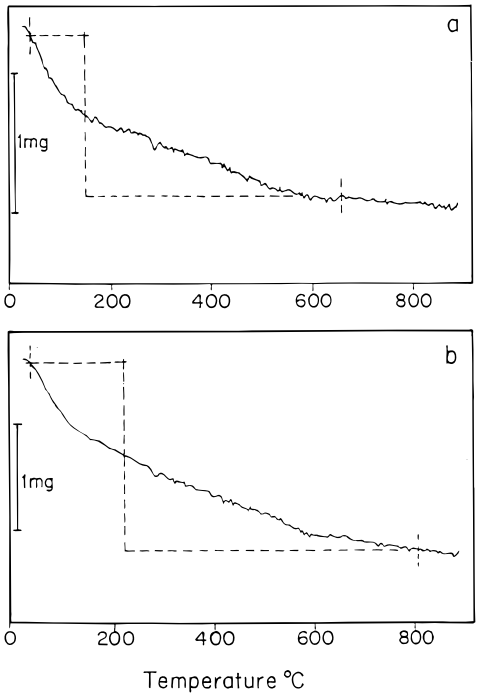

Figure 6. Thermogravimetric analysis (TGA) profiles of (a) the substrate silica microspheres (b) the as-prepared sample of silica deposited with nanophasic amorphous cobalt.

silanols on the inner pore walls. The condensation of silanols on the inner pore walls is not complete, as will be discussed in detail shortly, in the section on FT-IR spectroscopy. The liberation of these species from the inner walls is a diffusion-controlled process, and the process continues at a linear rate of weight loss up to 600 °C, after which no further weight loss is

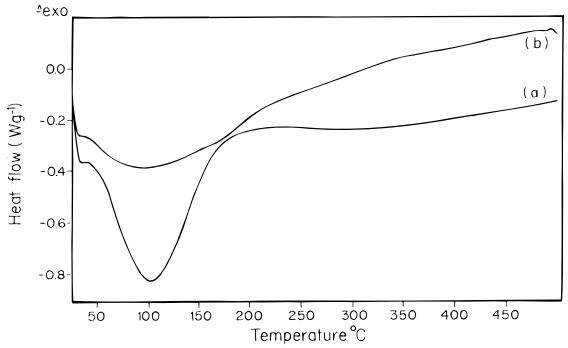

Figure 7. Differential scanning calorimetric (DSC) profiles of (a) the substrate silica microspheres (b) the as-prepared sample of silica deposited with nanophasic amorphous cobalt.

observed. The process is qualitatively the same in the case of silica samples covered with amorphous cobalt except that an additional higher weight loss of about 8%. Of this 8% about a 2% weight loss could be accounted for in the temperature range of 600−800 °C. The excess weight loss at lower temperatures can be accounted only by the desorption of the cobalt nitrosyl carbonyl precursor (see the section on IR spectroscopy) and the solvent decane adsorbed during sonication. Finally, a distinct weight loss in the temperature range of 600−800 °C, only in the case of cobalt-coated sample, can be accounted for by the loss of metallic cobalt itself, as it is unlikely that any organic impurity can be retained up to such high temperatures. On the other hand, cobalt metal itself is expected to have a finite vapor pressure, however small, in the temperature range of 600−800 °C and can account for the 2% weight loss, due to the evaporation of metal.

The breaking of the hydrogen-bonded network in the temperature range of 40−175 °C is reflected in the DSC trace as well. An endothermic peak in this range in the case of the substrate silica is due to the breaking up of the hydrogen-bonded network on silica. A lower heat of absorption in the case of silica covered with amorphous cobalt can originate from two effects: (a) The ultrasound radiation used for the deposition of cobalt itself is known[17] to disrupt the hydrogen-bonded network on bare silica microspheres, and (b) the adsorption of a zerovalent metal on a hydroxylated surface such as silica is known to form bonds of the $Si-O-M^{\delta+}$ type. Brenner and co-workers[24] studied the decarbonylation of various metal carbonyls of Mo, W, and Fe and the subsequent adsorption of zerovalent metals on the hydroxylated surfaces of silica and γ-Al_2O_3 and observed that the extent of oxidation of the metal was higher in the case of a hydroxylated surface and that zerovalent metals were normally oxidized at relatively low temperatures by the surface hydroxyls with the liberation of hydrogen. Formation of $Si-O-Co^{\delta+}$ type species on reaction with the surface silanols could further weaken the hydrogen-bonded network and contribute to the observed loss in the heat of adsorption.

(c) IR Absorption. Figure 8. shows the FT-IR spectra of (a) the bare substrate silica spheres, (b) the as-prepared cobalt-coated silica spheres, (c) the silica spheres carrying crystallized cobalt nanoparticles, and (d) the residue of the TGA run on the amorphous cobalt- coated silica particle carried up to a temperature of 900 °C under flowing nitrogen. As-prepared samples of amorphous cobalt on silica showed carbonyl stretches above 2000 cm^{-1} (marked as curve b) as evidence of the presence of small amounts of organometallic precursor or carbon monoxide readsorbed on the metal clusters.

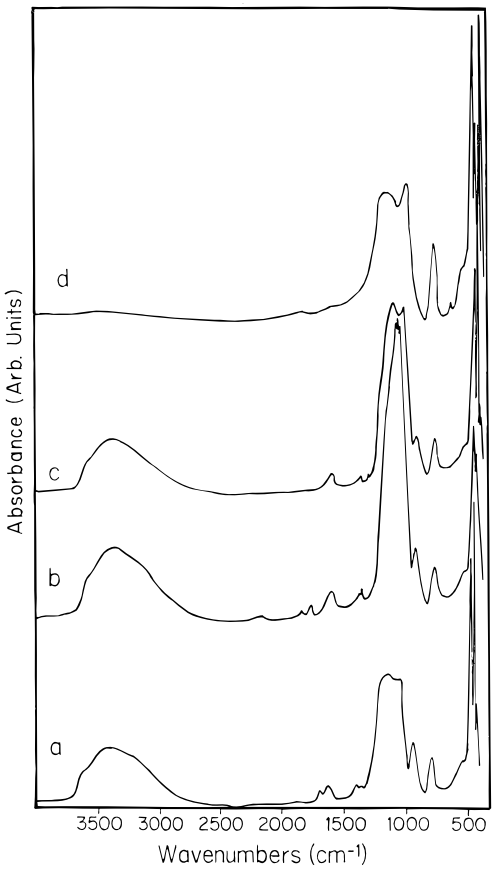

Figure 8. FT-IR spectra of (a) the bare substrate silica spheres (b) as prepared, amorphous cobalt-coated silica spheres (c) silica spheres carrying nanocrystalline cobalt and (d) the residue of the TGA run on the amorphous cobalt coated silica particle carried up to a temperature of 900 °C under flowing nitrogen.

All the samples except d showed the presence of intact surface silanols and hydrogen-bonded water absorbing in the 2800−3800 cm^{-1} range. The sample heated to 900° C (curve d) showed a complete absence of absorption above 2000 $cm.^{-1}$ Oxidation of the elemental metal by the surface silanols is influenced by the redox characteristics of the metal ion and the degree of hydroxylation of the surface. In our earlier investigations[14,18] on the interaction of amorphous metal clusters of nickel and iron with the spherical silica, IR absorptions of the various reactive species on the surface of silica were used to assess the extent of interaction between the metal and the surface. We observed that elemental nickel could be deposited even on a hydrated surface, whereas iron clusters were extremely reactive to yield various iron oxides dependent on the degree of hydroxylation. Burneau et al.[25] have listed the characteristic absorption bands for the precipitated silicas. Precipitated silica normally does not have free outer surface silanols which absorb at 3730−3740 cm^{-1}. The other two reactive species of bound outer silanols and silanols hydrogen bonded to adsorbed water absorb at 3520 and 3200 cm^{-1}, respectively. A fall in intensity of the peak at 3200−3300 cm^{-1}, observed in the case of iron-silica interaction, was not significant in the case of silica. The cobalt-coated sample heated at 400 °C for 3 h still contained significant hydroxyls and adsorbed water (on the inner pore walls), as could be verified from an intense absorption in the 3000−3500 cm^{-1} range. Removal of water due to condensed silanols was complete only when the sample was heated to a temperature of 800 °C (see curve d).

(d) Magnetic Properties. Magnetic properties were investigated by magnetic susceptibility and ferromagnetic resonance

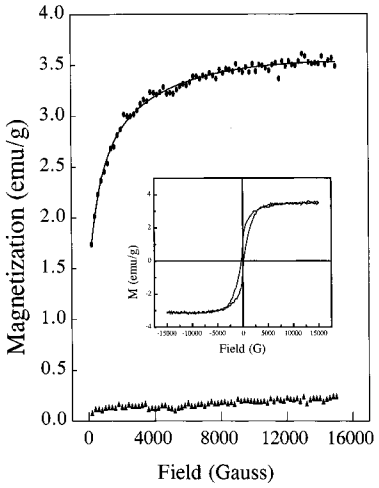

Figure 9. Field dependent magnetization of as prepared cobalt coated silica (shown as triangles) and (b) silica spheres carrying nanocrystalline cobalt (shown as circles). The solid line is the magnetization values calculated from the expression $M_H = M_{0,\,RT}\{1 - (\sigma_1/\sqrt{H}) - (\sigma_2/H) - (\sigma_3/\sqrt{H^3}) - ...\}$. Inset shows the hysteresis loop exhibited by silica microspheres carrying ferromagnetic cobalt nanocrystals.

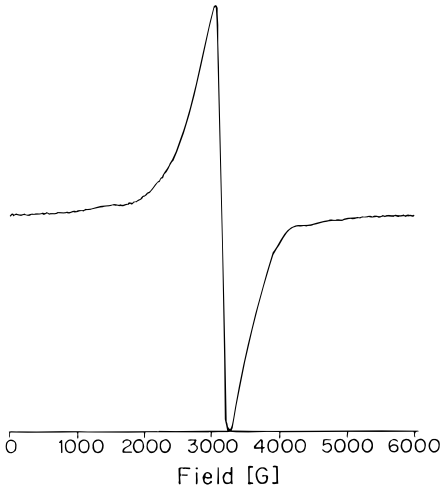

Figure 10. Electron paramagnetic resonance (EPR) exhibited by silica microspheres deposited with nanophasic amorphous cobalt clusters.

methods as outlined in the Experimental Section. The M−H curves for the as-prepared cobalt coated silica and the crystallized sample are shown in Figure 9. The amorphous cobalt clusters on silica showed a magnetization of about 0.25 (emu/g), inclusive of the diamagnetic silica core, and did not exhibit any hysteresis. On the other hand the crystallized samples of cobalt on amorphous silica showed a magnetization of about 3.5 emu/g inclusive of the silica core. Taking into account the weight of cobalt present in the entire material (from EDAX), the saturation magnetization of the nanocrystalline cobalt particles works out to approximately 70 emu/g. This material also exhibited a narrow hysteresis loop characteristic of ferromagnetically ordered materials. The hysteresis loop is shown as an inset in Figure 9. It is known that irreversibility in magnetization is experienced even in amorphous solids below the blocking temperature. If this were the case, the amorphous cobalt clusters as well could have exhibited a hysteresis loop, which is clearly not the case. However, the nature of magnetic ordering will shortly be discussed in terms of magnetic resonance properties as well. The diamagnetic contribution from the silica core to the total magnetization could not be ignored and this was calculated by a method described by Wang et al.[26]

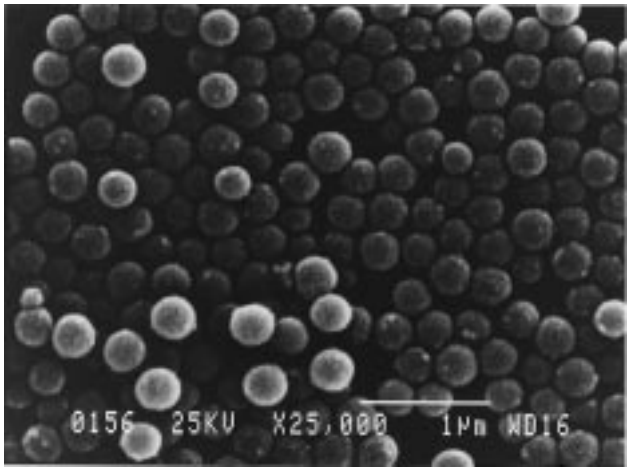

Figure 11. Scanning electron micrograph of silica microspheres carrying ferromagnetic cobalt nanoparticles, organized on a single crystalline Si⟨100⟩ surface.

The experimentally observed magnetization values as a function of applied field (H) were fitted to the expression.

$$M_H = M_{0,RT}\{1 - (\sigma_1/\sqrt{H}) - (\sigma_2/H) - (\sigma_3/\sqrt{H^3}) - ...\} + \phi_1\sqrt{H} + \phi_2 H \quad (3)$$

by a method of nonlinear regression by least-squares minimization. In eq 2, M_H is the observed magnetization, $M_{0,RT}$ is the magnetization value at room temperature, H is the field strength expressed in Oersteds, and σ_i, ϕ_i are the coefficients which give information about the magnetization processes at the interface. The regression yielded a satisfactory fit only in the case of nanocrystalline cobalt on silica, and the calculated value of magnetization is plotted as a solid line. The values of the calculated interfacial magnetization were $\sigma_1 = 14.03$, $\sigma_2 = -91.4$, $\phi_1 = 0.0091$, and $\phi_2 = -4.63 \times 10^{-5}$, respectively. The low magnetization values of about 4 emu/g (excluding the weight of the silica core) and the failure to attain saturation in the case of as-deposited cobalt originates from the amorphous nature of cobalt. It is a well-known phenomenon that for ferromagnetic metals, when divided into nanoparticles, the ferromagnetic ordering of the domains is lost to form particles exhibiting superparamagnetism.[27−29] The crystallized samples showed a saturation magnetization of about 3.5 emu/g, with a diamagnetic silica core accounting for a saturation magnetization of about 70 emu/g (based on cobalt content only). A negative value of the coefficient ϕ_2 is identified with a diamagnetic contribution from the silica core. However, the magnitude of the coefficient at 4.6×10^{-5} compared against a value of 1.42×10^{-3} in the case of Ni/SiO_2 interface[14] and -1.25×10^{-3} in the case of α-Fe/SiO_2 interface[18] suggests that diamagnetic contribution may be weaker in the case of cobalt nanocrystals as compared to nickel and iron nanocrystals adhered to spherical silica surface.

The resonance spectrum of the as-prepared cobalt coated sample is shown in Figure 10. The sample showed a peak to peak width (ΔH_{pp}) of 200 G and a g value of 2.1508. The crystalline sample was highly ferromagnetic that a resonance spectrum could not be recorded under identical conditions, even with least possible amount of sample. A sharp and narrower paramagnetic resonance signal (width 200 G) can be associated with the superparamagnetic nature of the as prepared cobalt nanoparticles. The experimental g value of 2.151 for these particles is slightly lower than a value of 2.187 reported for

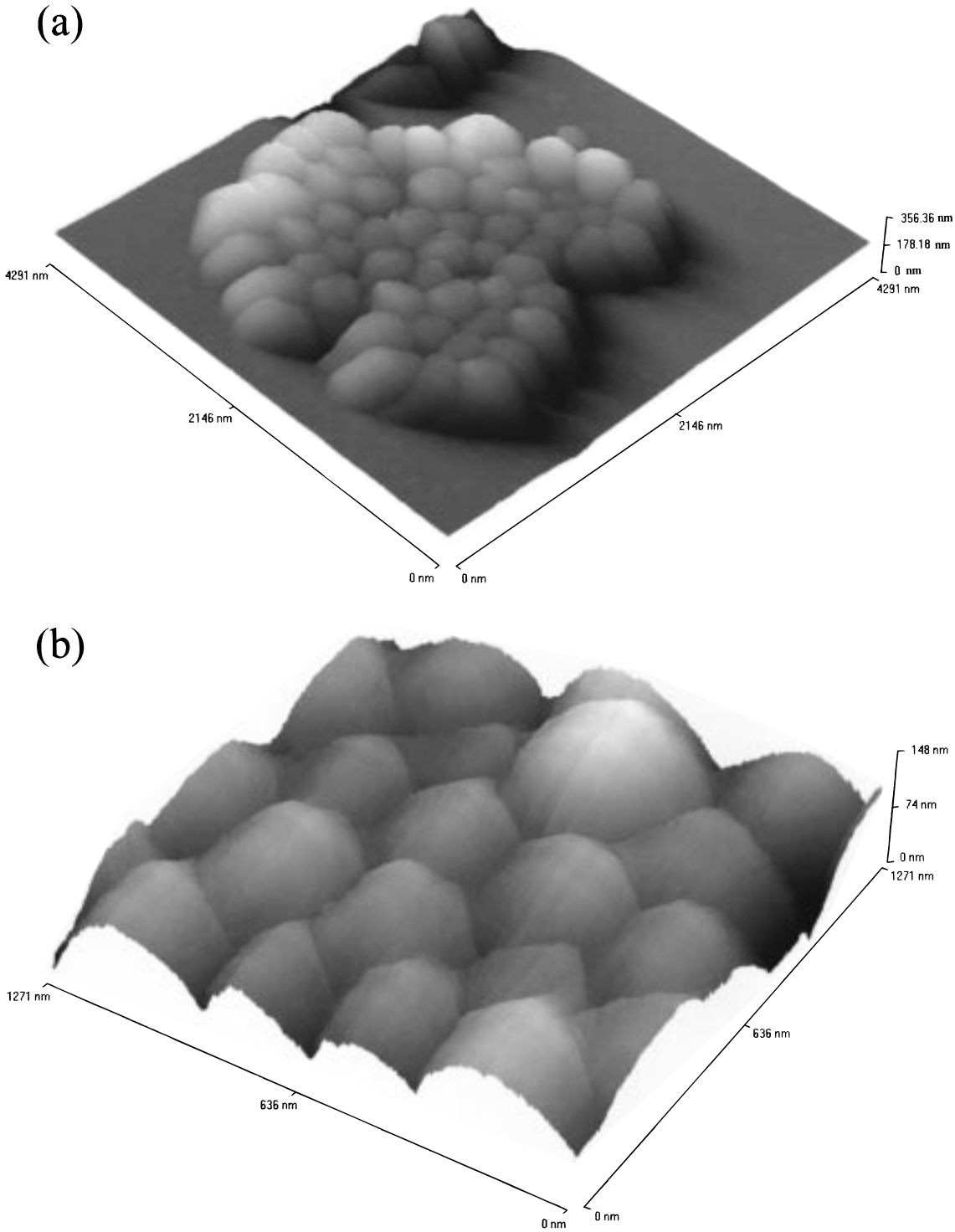

Figure 12. The AFM topographic image of (a) a monolayer of silica microspheres carrying ferromagnetic cobalt nanoparticles, organized on a single crystalline Si⟨100⟩ surface and (b) a high magnification image recorded on a section of the monolayer.

bulk cobalt[30] which could be linked to an infinitesimally positively charged cobalt metal in $Si-O-Co^{\delta+}$ type species.

(e) Organized Microspheres on Silicon. The scanning electron micrograph of a section of the organized silica microspheres carrying ferromagnetic cobalt nanoparticles on a single crystalline silicon surface is shown in Figure 11. Though a monolayer was formed on the surface of silicon, a few silica spheres on a second layer (brighter spheres) could also be seen on the first layer of the spheres. Normally such a monolayer of smaller spherical particles (50 nm) could be assembled at an air−liquid interface and transferred to a single crystalline substrate over large surface areas. Kondo et al.[31] fabricated monolayer arrays of silica particles modified by various surfactants by slowly evaporating a thin film formed at the air liquid interface. They found that the ordering toward monolayer formation was facilitated only when the interparticle attractions were weakened by suitable surfactants. For similar reasons only aggregates were formed among the 250 nm sized particles in the present case when an ethanolic solution was evaporated in the absence of spinning. The 3D AFM topographic image of silica monolayers and a closer view at a section of the monolayer are shown in Figure 12a and b, respectively. The distortions caused due to the interactions with the sides of a pyramidal AFM tip on the image of the spherical particles at the boundary

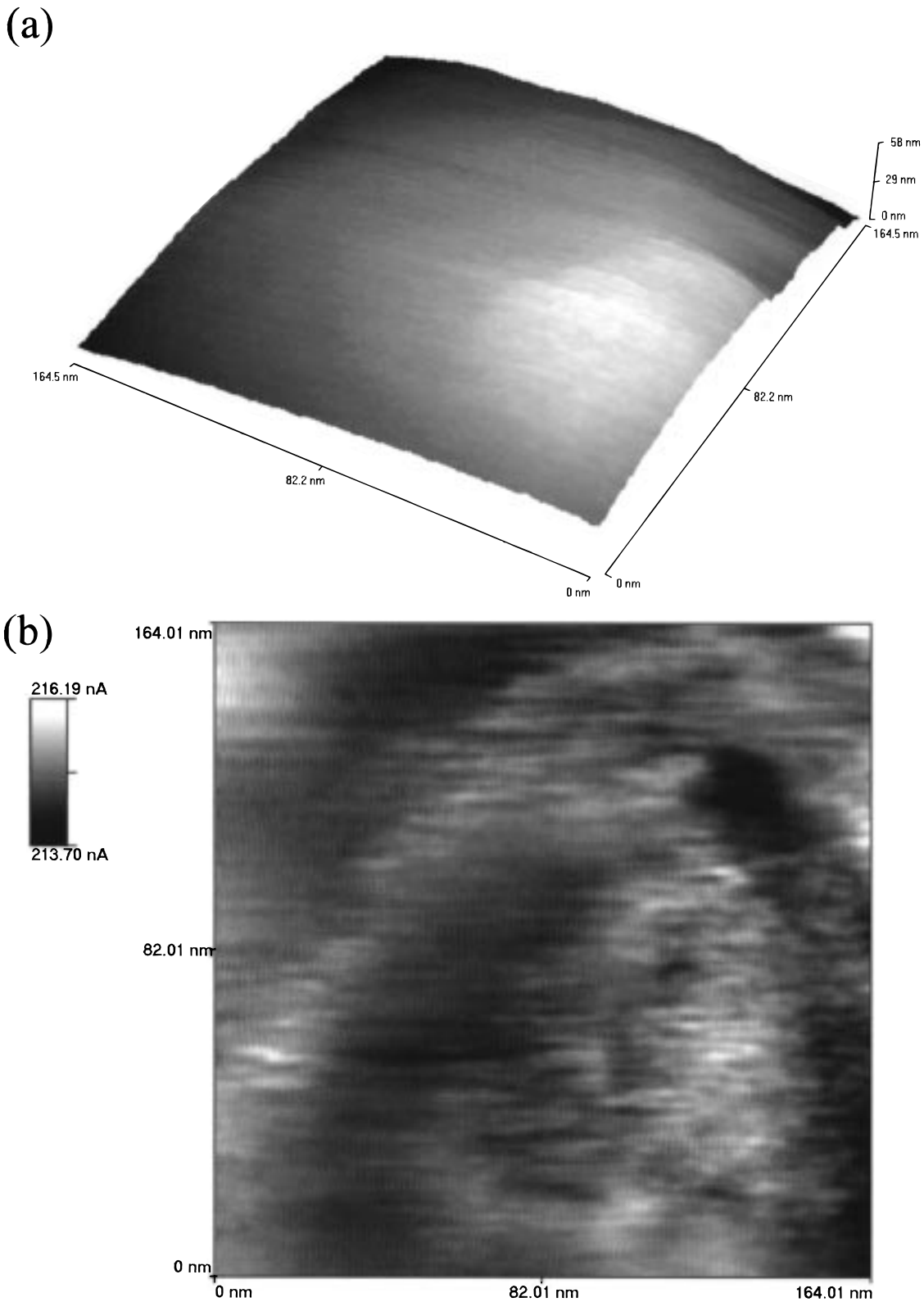

Figure 13. (a) The three-dimensional topographic image of a single cobalt-coated silica sphere immobilized in a thermoplastic resin bed. (b) The corresponding two-dimensional lateral force map.

could be seen in Figure 12a. The microsopheres were firmly fixed to the silica substrate and allowed topographic imaging without any tip-induced surface movements[32] or damaging of the surface[33] as is the case with weakly adhered or soft sample particles. However the cobalt nanoparticles adhered to the silica microspheres could not be imaged due to an uniform coating of gold on the monolayer of the microspheres. However, the nature of adhesion of the ferromagnetic particles were examined in a lateral force mode on single microspheres immobilized in a thermoplastic resin bed. Figure 13a shows the three-dimensional topographic image of the surface of a single silica sphere carrying cobalt nanocrystals. The cobalt particles were imaged in lateral force mode as can be seen from the corresponding lateral force map shown in Figure 13b. The cobalt nanoparticles could be imaged, signifying negligible tip-induced movements of cobalt nanocrystals on single microspheres.

In a recent AFM investigation[19] we compared the adhesion of as prepared amorphous and crystallized nickel nanoparticles to the surface of submicrospherical silica and found that the amorphous particles underwent huge tip induced surface movements due to poor adhesion. On the other hand lateral force imaging of individual metal nanoparticles on a single silica microsphere is possible only when the metal particles were firmly adhered to the silica surface.

Conclusions

Hard, microspherical substrates carrying magnetic nanoparticles can be organized in two-dimensional arrays on single crystalline substrates. Sonochemical deposition methods taken together serve as a single-step tool to synthesize ferromagnetic nanoparticles from organometallic precursors and deposit them on isotropic substrates placed in a suspension. As-prepared cobalt nanoclusters were superparamagnetic and had to be crystallized at 400 °C to obtain ferromagnetic nanocrystals. The interfacial magnetization coefficients evaluated from the field-induced magnetization showed a diamagnetic contribution from the silica core to the net magnetization, though to a lesser extent, compared to $Ni-SiO_2$ or $Fe-SiO_2$ systems. Interparticle attractions were overcome by centrifugal forces to form ordered two-dimensional arrays on single crystalline $Si\langle 100\rangle$ surface. The cobalt nanocrystals were strongly adhered to the silica core to allow lateral force imaging without tip induced surface movements. With silica microspheres of radius $r_1 = 250$ nm and $r_2 = 125$ nm (as in the present case) and for a cobalt magnetic particle of 10 nm diameter, the scanning area diameter works out to be 300 nm as per eq 2 at a separation distance (δ) of 5 nm.

Acknowledgment. A. Gedanken thanks the Ministry of Science for supporting this research through the grants for infrastructure. The authors thank Prof. M. Deutsch for extending the XRD facility. Thanks are due to Prof. Yeshurun for extending the facilities of National center for magnetic measurements. R.P thanks Clore foundation for a fellowship. The authors also thank Dr. Shifra Hochberg for editorial assistance.

References and Notes

(1) Fendler, J. H. *Membrane-Mimetic Approach to Advanced Materials*; Springer-Verlag: Berlin, 1994.

(2) (a) Murray, C.; Kagan, C.; Bawendi, M. *Science* **1995**, *270*, 1335. (b) Dimitrov, A. S.; Nagayama, K. *Langmuir* **1996**, *12*, 1303. (c) Fulda, K. U.; Ticke, B. *Adv. Mater*. **1994**, *6*, 288. (d) Graber, K. C.; Freeman, R. G.; Hommer, M. B.; Natan, M. J. *Anal. Chem*. **1995**, *67*, 735. (e) Tian, Y.; Wu, C.; Fendler, J. H. *J. Phys. Chem.* **1994**, *98*, 4913. (f) Cusack, L.; Rizza, R.; Gorelov, A.; Fitzmaurice, D. *Angew. Chem., Int. Ed. Engl.* **1997**, *36*, 848. (g) Hillmyer, M. A.; Lipic, P. M.; Hajuduk, D. A.; Almdal, K.; Bates, F. S. *J. Am. Chem. Soc.* **1997**, *119*, 2749. (h) Harfenist, S. A.; Wang, Z. L.; Alvarez, M. M.; Vezmar, I.; Whetten, R. L. *J. Phys. Chem*. **1996**, *100*, 13904. (i) Sato, T.; Brown, D.; Johnson, B. F. G. *Chem. Commun*. **1997**, 1007.

(3) Evans, G. T. *J. Chem. Phys*. **1997**, *106*, 9718 and references therein.

(4) Burmeister, F.; Schafle, C.; Matthes, T.; Bohmisch, M.; Boneberg, J.; Leiderer, P. *Langmuir* **1997**, *13*, 2983.

(5) Demaille, C.; Brust, M.; Tsionsky, M.; Bard, A. J. *Anal. Chem*. **1997**, *69*, 2323.

(6) (a) Holtz, J. H.; Asher, S. A. *Nature* **1997**, *389*, 829. (b) Pan, G.; Kesavamoorthy, R.; Asher, S. A. *Phys. Rev. Lett.* **1997**, *78*, 3860.

(7) (a) Holland, B. T.; Blanford, C. F.; Stein, A. *Nature* **1998**, *281*, 538. (b) Antonietti, M.; Berton, B.; Goltner, C.; Hentze, H. P. *Adv. Mater*. **1998**, *10*, 154.

(8) Sarid, D. *Scanning Force Microscopy*; Oxford University Press: New York, 1994.

(9) Di Nardo, N. J. *Nanoscale Characterization of Surfaces and Interfaces*; VCH: Germany, 1994.

(10) Wadas, A.; Grutter, P. *Phys. Rev. B* **1989**, *39*, 12013.

(11) Drexler, K. E. *Nanosystems: Molecular Machinery, Manufacturing and Computation;* John-Wiley & Sons: New York, 1992; pp 459.

(12) Drexler, K. E.; Foster, J. S. *Nature* **1990**, *343*, 600.

(13) (a) Cao, X.; Koltypin. Yu.; Kataby, G.; Prozorov, R.; Gedanken, A. *J. Mater. Res*. **1995**, *10*, 2952. (b) Koltypin, Yu.; Katabi, G.; Prozorov, R.; Gedanken, A. *J. Non-Cryst. Solids.* **1996**, *201*, 159. (c) Cao, X., Prozorov, R.; Koltypin, Yu.; Kataby, G.; Gedanken, A. *J. Mater. Res*. **1997**, *12*, 402 (d) Shafi, K. V. P. M.; Koltypin, Yu.; Gedanken, A.; Prozorov, R.; Balogh, J.; Lendavi, J.; Felner, I. *J. Phys. Chem. B* **1997**, *101*, 6409.

(14) Ramesh, S.; Koltypin, Y.; Prozorov, R.; Gedanken, A. *Chem. Mater*. **1997**, *9*, 546.

(15) Suslick, K. S., Ed. *Ultrasound: Its Chemical, Physical and Biological Effects*; VCH Publishers, Germany, 1988.

(16) Stober, W.; Fink, A.; Bohn, E. *J. Colloid Interface Sci.* **1968**, *26*, 62.

(17) (a) Ramesh, S.; Koltypin, Y.; Gedanken, A. *J. Mater. Res*. **1997**, *12*, 3271. (b) Ramesh, S.; Sominska, E.; Cina, B.; Chaim, R.; Gedanken, A. *J. Am. Ceram. Soc*. **1998**. In press.

(18) (a) Ramesh, S.; Prozorov, R.; Gedanken, A. *Chem. Mater*. **1997**, *9*, 2996. (b) Ramesh, S.; Felner, I.; Koltypin, Y.; Gedanken, A. Private communication.

(19) Ramesh, S.; Cohen, Y.; Aurbach, D.; Gedanken, A. *Chem. Phys. Lett.* **1998**, *287*, 461.

(20) Job, R.; Rovang, J.; *Synth. Reac. Inorg. Metal-Org. Chem*., **1976**, *6*, 367.

(21) Tsuchiya, I. *J. Phys. Chem.* **1982**, *86*, 4107.

(22) Kondo, S.; Muroya, M.; Fujii, K. *Bull. Chem. Soc. Jpn.* **1974**, *47*, 553.

(23) Chuang, I. S.; Maciel, G. E. *J. Am. Chem. Soc.* **1996**, *118*, 401.

(24) (a) Brenner, A.; Hucul, D. A.; Hardwick, S. J. *Inorg. Chem*. **1979**, *18*, 1478. (b) Brenner, A.; Hucul, D. A. *Inorg. Chem*. **1979**, *18*, 2836. (c) Hucul, D. A.; Brenner, A. *J. Phys. Chem*. **1981**, *85*, 496.

(25) Burneau, A.; Barres, O.; Gallas, J. P.; Lavalley, J. C. *Langmuir* **1990**, *6*, 1364.

(26) Wang, W. N.; Cheng, G. X.; You, W. D. *J. Magn. Magn. Mat*. **1996**, *153*, 11.

(27) Kaneyoshi, T. *Amorphous Magnetism;* CRC Press: Boca Raton, Florida, 1984.

(28) Jiao, J.; Seraphin, S.; Wang, X.; Withers, J. C. *J. Appl. Phys*. **1996**, *80*, 103.

(29) (a) Osuna, J.; de Caro, D.; Amiens, C.; Chaudret, B.; Snoeck, E.; Respaud, M.; Broto, J. M.; Fert, A. *J. Phys. Chem*. **1996**, *100*, 14571. (b) Grinstaff, M. W.; Salamon, M. B.; Suslick, K. S. *Phys. Rev. B* **1993**, *48*, 269. (c) Chen, J. P.; Lee, K. M.; Sorensen, C. M.; Klabunde, K. J.; Hadjipanayis, G. C. *J. Appl. Phys*. **1994**, *75*, 5876.

(30) Wohlfarth, E. P. In *Ferromagnetic Materials*; Wohlfarth, E. P., Ed.; North-Holland: Amsterdam, 1980; Vol. I.

(31) Kondo, M.; Shinozaki, K.; Bergstrom, L.; Mitzutani, N. *Langmuir* **1995**, *11*, 394.

(32) Roberts, C. J.; Wilkins, M. J.; Beamson, G.;. Davies, M. C.; Jackson, D. E.; Scholes, P. D.; Tendler, S. J. B.; Williams, P. M. *Nanotechnol*. **1992**, *3*, 98.

(33) Unertl, W. N.; Jin, X.; White, R. C. In *Polyimides and other High-temperature Polymers;* Elsevier: Amsterdam, 1991.